IEEE Access
Multidisciplinary | Rapid Review | Open Access Journal

Received December 18, 2018, accepted January 6, 2019, date of publication January 16, 2019, date of current version February 4, 2019.

Digital Object Identifier 10.1109/ACCESS.2019.2891889

High-Order Planar Bandpass Filters With Electronically-Reconfigurable Passband Width and Flatness Based on Adaptive Multi-Resonator Cascades

ROBERTO GÓMEZ-GARCÍA[1], (Senior Member, IEEE), JOSÉ-MARÍA MUÑOZ-FERRERAS[1], (Member, IEEE), JESÚS JIMÉNEZ-CAMPILLO[2], FEDERICO BRANCA-RONCATI[2], AND PETRONILO MARTÍN-IGLESIAS[3]

[1]Department of Signal Theory and Communications, University of Alcalá, 28871 Alcalá de Henares, Spain
[2]Thales Alenia Space España, 28760 Tres Cantos, Spain
[3]European Space Research and Technology Centre, European Space Agency, 2201 Noordwijk, The Netherlands

Corresponding author: Roberto Gómez-García (roberto.gomez.garcia@ieee.org)

This work was supported by the Project Compact Tunable IF Filters granted by the European Space Agency under Grant ITT ESA AO/1-8275/15/NL/HK.

ABSTRACT A class of quasi-elliptic-type planar bandpass filters (BPFs) with electronically controllable bandwidth between narrow-band and ultra-wideband states and enhanced passband flatness is reported. It consists of the in-series cascade of replicas of an adaptive BPF stage that exhibits three in-band poles and two transmission zeros (TZs). In this manner, BPF transfer functions with $3K$ poles and multiple TZs—between two K-multiplicity and $2K$ one-multiplicity TZs—without cross-coupling can be synthesized with a K-stage BPF architecture. Bandwidth reconfiguration is performed through the spectrally agile allocation of these TZs. Passband flattening for all the states is accomplished through the adjustment of the BPF in-band return-loss profile by tuning the external admittance inverters and those between BPF stages. The aforementioned procedures for bandwidth control and passband flattening are theoretically demonstrated with the coupling–routing diagram formalism. Furthermore, a mechanism to avoid the appearance of out-of-band spurious peaks due to the multi-stage in-series-cascade process in the associated transmission-line-based BPF implementation is described. For experimental-validation purposes, a 1-GHz sixth-order varactor-tuned BPF microstrip prototype with measured flattened 1-dB referred passband-width states going from 46 to 482 MHz—measured bandwidth tuning ratio of 11.5:1—is developed and characterized. Measurements for various temperature conditions and their *in situ* compensation are also shown.

INDEX TERMS Bandpass filter (BPF), bandwidth control, electronically-controllable filter, intermediate-frequency (IF) filter, microstrip filter, multi-functional filter, passband flattening, reconfigurable filter, satellite-communication receiver, transmission zero (TZ), tunable filter, varactor-tuned filter.

I. INTRODUCTION

Next-generation satellite-communication receivers demand advanced microwave and intermediate-frequency (IF) electronics with reduced volume/size and capable of operating for different signal conditions [1], [2]. In the case of bandpass filters (BPFs) and multiplexing devices as they are the basic signal-preselection components for such systems, the future trend is to replace—when possible—bulky waveguide- and cavity-resonator-based frequency-static BPFs and switchable-filter-banks/channelizers by planar implementations. Nevertheless, planar technologies, such as microstrip and stripline, apart from their lower power-handling capability, exhibit a much-lower quality factor when compared to waveguide/cavity-resonator-based BPF structures. This results in higher in-band power insertion loss and selectivity degradation—including a passband-rounding effect with subsequent amplitude-distortion problems for in-band processed signals—as the BPF bandwidth is decreased.

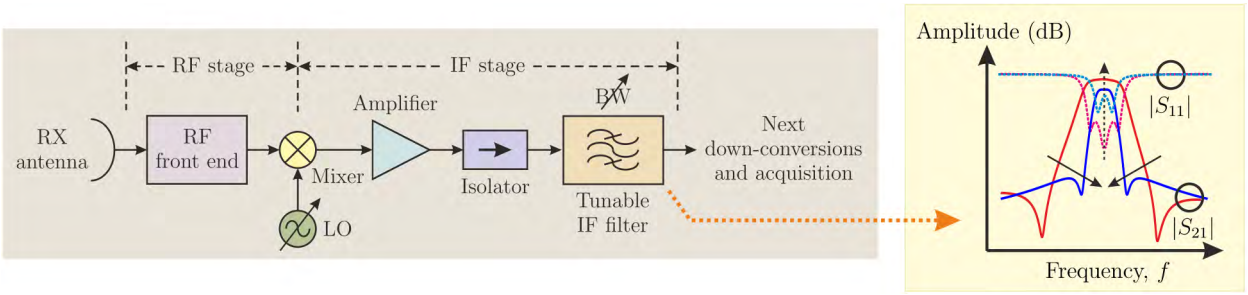

FIGURE 1. Block diagram of the RF and IF stages of a potential future satellite-communications receiver architecture using a bandwidth/amplitude-flatness-tunable IF filter (RF: radiofrequency; IF: intermediate frequency; RX: receiver; BW: bandwidth; LO: local oscillator).

Whereas lossy and predistorted BPF design techniques have been proposed as an effective solution to increase the effective quality factor at the expense of higher in-band power-insertion loss and/or power-reflection levels, they have been mainly exploited in frequency-static BPF realizations [3]–[7]. Hence, there is now a lack of frequency-reconfigurable BPF architectures with simultaneous in-band-amplitude-flattening capabilities for different transfer-function states.

The purpose of this work is to research on a compact IF tunable-bandwidth BPF for a flexible satellite-communication receiver with highly-adaptive passband-width—bandwidth-tuning ratio larger than 10:1—and in-band amplitude-flattening capabilities for all the states. Fig. 1 depicts the block diagram of a potential future satellite-communication receiver in which such a filtering device may be exploited as the replacement of a switchable filter bank with individuals BPFs for each state. Whereas a tunable local oscillator (LO) allows to situate any received RF signal at the same IF after mixing, the IF bandwidth-tunable BPF allows to select different-nature signals—from narrow-band to-ultra-wideband signals that may correspond to multiple services—with minimized amplitude-distortion effects due to the passband flattening. Furthermore, undesired signal-power reflections caused by the in-band flattening would be efficiently absorbed by the isolator at its input to protect the preceding amplifier.

Over the last years, several principles to design bandwidth-controllable BPFs in planar technologies have been proposed. These solutions can be grouped into different categories, as follows: (i) BPFs based on single-resonance-coupled-resonator networks with variable couplings, (ii) BPFs based on frequency-controllable signal-interference techniques, (iii) BPFs based on controllable multi-mode resonators, and (iv) BPFs based on adaptive transmission-zero-(TZ)-generation cells. Whereas the use of variable couplings in mono-mode-resonator circuit networks were adopted as one of the initial approaches for bandwidth tuning in BPFs, they are mostly valid for narrow-to-moderate variable-bandwidth designs [8]–[14]. The exploitation of adaptive signal-interference principles to obtain bandwidth-controllable sharp-rejection filtering actions has also been proven, but for discretely-selectable moderate-to-ultra-wide passband-width states in relatively-large circuits [15], [16]. Bandwidth-tunable multi-mode-resonator-based BPFs have shown large bandwidth-tuning ratios up to 8:1, but they suffer from effective-quality-factor degradation for narrow-band states [17]–[20]. On the other hand, similar limitations can be found in adaptive-resonator-cascade-based BPFs along with the appearance of out-of-band spikes and spurious bands in some cases [21]–[24], or in terms of basic discrete control for other types of reconfigurable-filtering-section cascades [25]. Hence, to the best of the authors' knowledge, no bandwidth-tunable BPF with a bandwidth-tuning ratio larger than 10:1 between narrow-band and ultra-wideband states and synchronous passband-flattening capabilities has been proposed.

A class of bandwidth-reconfigurable quasi-elliptic-type BPF with simultaneous passband-flatness control is reported in this paper. The conceived adaptive BPF approach, which exploits a multi-resonator-cascade arrangement, allows to configure the passband-width between narrow-band and ultra-wideband states with in-band flatness enhancement by means of a frequency-selective reflection process of the in-band input signal. With regard to the preliminary work presented by Gómez-García *et al.* [26] for low-order BPF designs, this expanded paper presents the following new contents: (i) extrapolation of the concept to higher-order BPF realizations through multi-stage in-series-cascade architectures, (ii) complete coupling-routing-diagram-based study of the conceived bandwidth-control and in-band flattening mechanisms for quasi-equiripple BPF designs, (iii) new technique to avoid the presence of the undesired out-of-band spikes due to the multi-stage cascading process that were observed in other previous related works (e.g., [21], [27]), and (iv) manufacturing and testing of a novel electronically-tunable two-stage microstrip BPF prototype with six poles and four TZs that can be grouped as two double TZs below and above the passband.

The rest of the manuscript is organized as follows: in Section II, the coupling-routing-diagram foundations of the proposed bandwidth-control and in-band-flattening mechanisms in BPF architectures with one and multiple

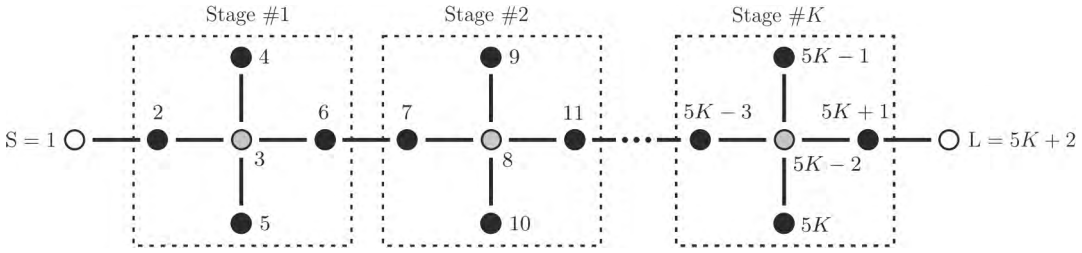

FIGURE 2. Normalized coupling-routing diagram of the K-stage adaptive-bandwidth/enhanced-in-band-flatness BPF concept ($K \geq 1$) [black circles: resonating nodes; gray circles: zero-susceptance non-resonating nodes (NRNs); white circles: unitary source (S) and load (L); continuous lines: couplings; and Ω: normalized frequency].

stages are described. Here, design aspects related with the capacitively-loaded transmission-line implementation of this BPF principle are described. Section III reports the simulated and measured results of a manufactured varactor-tuned two-stage microstrip BPF prototype at 1 GHz for practical-demonstration purposes, including its testing in different temperature conditions. Finally, a summary and the most relevant conclusions of this work are provided in Section IV.

II. OPERATIONAL FOUNDATIONS OF THE PROPOSED RECONFIGURABLE FILTER CONCEPT

This section reports the theoretical principles of the conceived adaptive-bandwidth/enhanced-in-band-flatness BPF architecture. First, its coupling-routing diagram and its underlying bandwidth-control and passband-flattening mechanisms are described. Subsequently, a quasi-distributed-element realization suitable for this reconfigurable BPF approach based on a capacitively-loaded transmission-line arrangement is presented. Undesired phenomena associated to such BPF implementation, namely the generation of out-of-band spurious transmission peaks in its transfer function and a technique for their mitigation, are also expounded.

A. COUPLING-ROUTING DIAGRAM

The coupling-routing diagram of the proposed BPF with bandwidth-variation and passband-flattening capabilities—K-stage architecture—is shown in Fig. 2. As can be seen, it is made up of the in-series cascade connection of multiple replicas of a BPF stage. Each BPF stage consists of two in-line resonating nodes and one TZ-generation cell shaped by two resonating nodes that are coupled to a zero-susceptance non-resonating node (NRN) through different admittance inverters. This cell creates two TZs at the natural frequencies of its two resonating nodes and one in-band pole at the frequency at which the input admittances of its branches mutually cancel each other. In this manner, a $3K$-order BPF transfer function with multiple TZs—between two K-multiplicity and $2K$ one-multiplicity TZs—can be realized with the K-stage BPF structure in Fig. 2. In particular, for a symmetrical $3K$-pole BPF topology with a normalized filtering response centered at Ω_0 and lower and upper K-multiplicity TZs at Ω_{z1} and Ω_{z2}, respectively, the following conditions are imposed on its admittance-inverter and self-resonance coefficients ($\{M_{i,j}\}$ for the subindex values indicated below and $K \geq 1$):

$$M_{5k-3,5k-3} = M_{5k+1,5k+1} = -\Omega_0 \quad (1)$$

$$M_{5k-1,5k-1} = -M_{5k,5k} = -\Omega_z \quad (2)$$

$$M_{5k-2,5k-1} = M_{5k-2,5k} \quad (3)$$

$$M_{5k'-2,5k'-1} = M_{5(K-k')+3,5(K-k')+4} = K_{k'} \quad (4)$$

$$M_{5k'-4,5k'-3} = M_{5(K-k')+6,5(K-k')+7} \quad (5)$$

$$M_{5k'-3,5k'-2} = M_{5(K-k')+3,5(K-k')+6} \quad (6)$$

$$M_{5k'-2,5k'+1} = M_{5(K-k')+2,5(K-k')+3} \quad (7)$$

where $k = 1, 2, ..., K$, $k' = 1, 2, ..., \lceil K/2 \rceil$, and $\Omega_{z1} = -\Omega_{z2} = \Omega_z$.

For illustration purposes, the power transmission and reflection parameters of one-to-three-stage BPF examples that were theoretically synthesized through (1)–(7) are shown in Fig. 3—i.e., $K = 1, 2$, and 3. The indicated admittance-inverter and self-resonance coefficient values were derived from an optimization procedure aimed to obtain the same locations for the TZs—i.e., $\Omega_{z1} = -\Omega_{z2} = 5.5$—, an identical minimum in-band power-matching level of 20 dB, the same 1-dB-referred bandwidth of $\Omega_{1dB} = 6.2$, and a quasi-equiripple-type BPF profile. As can be seen in Fig. 3, the selectivity of the BPF increases with the number of stages K. In particular, the minimum out-of-band power-attenuation level for the one-, two-, and three-stage BPF design examples in Fig. 3 are 19.6 dB, 55.3 dB, and 91.6 dB, respectively.

The operational foundations for the bandwidth-control and passband-flattening mechanisms of the multi-stage BPF architecture in Fig. 2 are detailed below:

- Passband-width reconfiguration is performed by tuning the closest-to-passband TZs of the overall BPF transfer function through the resonating nodes of the TZ-generation cell that produce them. In this manner, narrower passband widths are obtained for more-closely-spaced TZs. Nevertheless, if the admittance inverters remain static, this is done at the expense of the deterioration of the in-band flatness as the bandwidth gets narrower. Moreover, this effect becomes even more prominent with the incorporation of the losses—i.e., finite quality factor—in the resonating nodes.

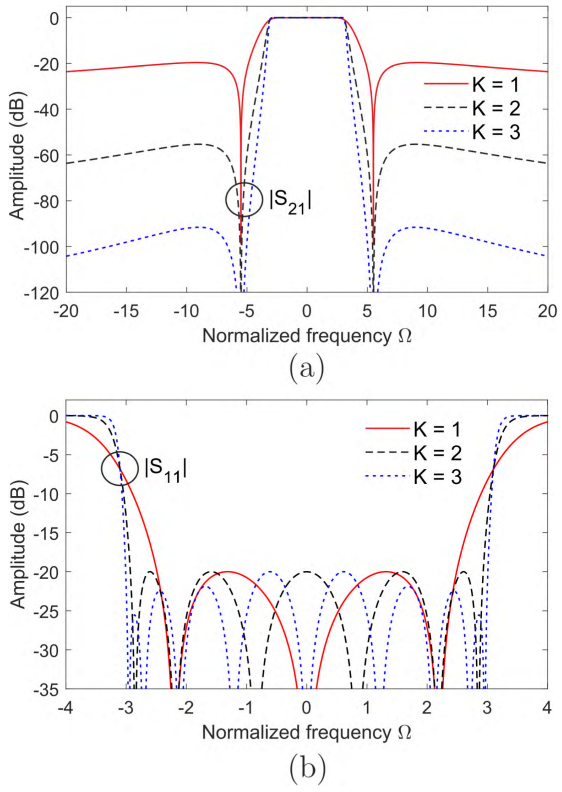

FIGURE 3. Theoretical power transmission ($|S_{21}|$) and reflection ($|S_{11}|$) parameters of ideally-synthesized one-, two-, and three-stage examples for the adaptive-bandwidth/enhanced-in-band-flatness BPF architecture in Fig. 2 ($K = 1$: $K_1 = 1.6510$, $M_{1,2} = M_{6,7} = 1.8746$, and $M_{2,3} = M_{3,6} = 1.3563$; $K = 2$: $K_1 = 1.6896$, $M_{1,2} = M_{11,12} = 1.9325$, $M_{2,3} = M_{8,11} = 1.3633$, $M_{3,6} = M_{7,8} = 0.9072$, and $M_{6,7} = 1.8281$; $K = 3$: $K_1 = 1.0559$, $K_2 = 1.5556$, $M_{1,2} = M_{16,17} = 2.0213$, $M_{2,3} = M_{13,16} = 0.9054$, $M_{3,6} = M_{12,13} = 0.5764$, $M_{6,7} = M_{11,12} = 1.8026$, and $M_{7,8} = M_{8,11} = 0.7434$; $\Omega_0 = 0$ and $\Omega_z = 5.5$ for all examples). (a) $|S_{21}|$. (b) $|S_{11}|$.

- Enhanced passband flatness for each bandwidth state can be realized by means of an in-band frequency-selective power-reflection process. This can be accomplished by adjusting the admittance inverters between the source and the first resonator, the load and the last resonator, and the ones that connect the different stages in the in-series-cascade BPF architecture.

Thus, tunable resonators in the TZ-creation cells of the BPF stages and variable source/load-to-first/last-resonator and inter-stage admittance inverters are utilized for the bandwidth-control and passband-flattening procedures, respectively. The aforementioned reconfiguration capabilities have been theoretically validated in the two-stage BPF version in Fig. 4 corresponding to the BPF scheme in Fig. 2 for $K = 2$. As can be seen, the resonating nodes responsible for the generation of the TZs vary their natural frequencies while satisfying (2)—i.e., $M_{4,4} = M_{9,9} = -M_{5,5} = -M_{10,10} = -\Omega_z$. Besides, to assure a high input/output in-band power matching for all the bandwidth states, the external and inter-stage admittance inverters—i.e., $M_{1,2} = M_{11,12}$ and $M_{6,7}$—need to be modified. Fig. 5 shows the theoretically-synthesized power transmission parameter of the two-stage

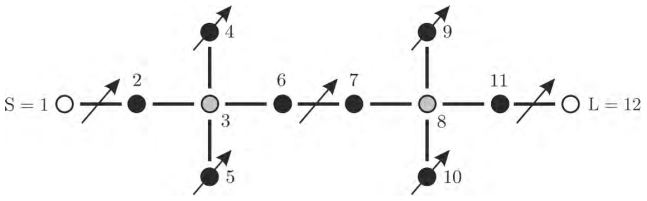

FIGURE 4. Normalized coupling-routing diagram of the two-stage ($K = 2$) adaptive-bandwidth/enhanced-in-band-flatness BPF architecture in Fig. 2 ($\Omega_0 = 0$, $K_1 = 1.6896$, $M_{2,3} = M_{8,11} = 1.3633$, and $M_{3,6} = M_{7,8} = 0.9072$; Ω_z, $M_{1,2} = M_{11,12}$, and $M_{6,7}$ are the reconfigurable variables).

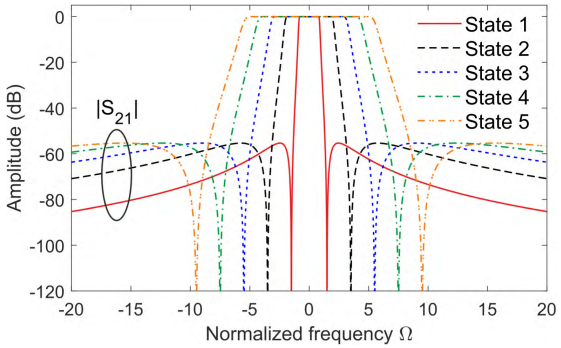

FIGURE 5. Theoretical power transmission ($|S_{21}|$) parameter of several states for the two-stage ($K = 2$) adaptive-bandwidth/enhanced-in-band-flatness BPF architecture in Fig. 4 (state 1: $\Omega_z = 1.5$, $M_{1,2} = M_{11,12} = 1.0092$, and $M_{6,7} = 0.4986$; state 2: $\Omega_z = 3.5$, $M_{1,2} = M_{11,12} = 1.5415$, and $M_{6,7} = 1.1634$; state 3: $\Omega_z = 5.5$, $M_{1,2} = M_{11,12} = 1.9325$, and $M_{6,7} = 1.8281$; state 4: $\Omega_z = 7.5$, $M_{1,2} = M_{11,12} = 2.2566$, and $M_{6,7} = 2.4929$; state 5: $\Omega_z = 9.5$, $M_{1,2} = M_{11,12} = 2.5397$, and $M_{6,7} = 3.1577$).

BPF design in Fig. 4 for several bandwidth states under these conditions. All these lossless-filter responses exhibit a minimum out-of-band power-rejection level of 55.3 dB and a six-pole equiripple-type power-reflection parameter with a minimum in-band power-matching level of 20 dB. On the other hand, for one of these states, Fig. 6 demonstrates the passband-rounding effect due to the addition of the losses in the resonating nodes, as well as how the passband flatness can be restored by readjusting the variable admittance inverters. However, this is done at the expense of increased in-band power-reflection loss—from 20 dB to 8.5 dB—like in conventional predistortion techniques for static BPFs.

Finally, it should be remarked upon that a large variety of out-of-band attenuation profiles can be realized by tuning the TZs of each BPF stage in an asynchronous way. This is illustrated in Fig. 7, which depicts the theoretical power transmission and reflection parameters for an example state of the two-stage BPF configuration in Fig. 4 with four TZs.

B. CAPACITIVELY-LOADED TRANSMISSION-LINE REALIZATION AND CONSIDERATIONS

The previously-described coupling-routing diagram in Fig. 2 of controllable-bandwidth/passband-flatness BPF can be realized by means of different microwave-circuit structures. Owing to the frequency dependance of the specific

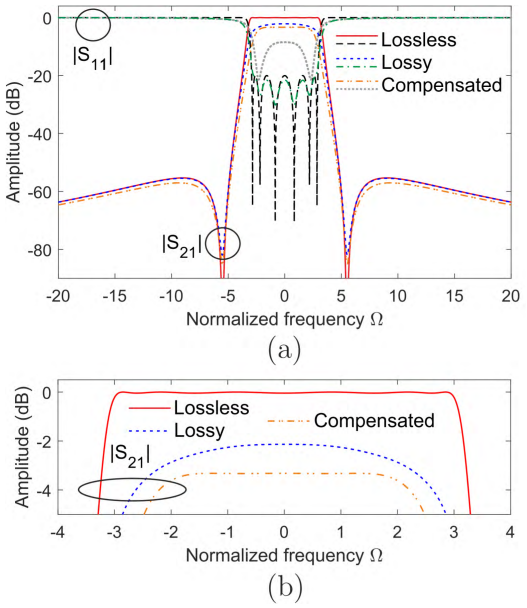

FIGURE 6. Theoretical power transmission ($|S_{21}|$) and reflection ($|S_{11}|$) parameters of the two-stage ($K = 2$) adaptive-bandwidth/enhanced-in-band-flatness BPF architecture in Fig. 4 with demonstration of in-band flatness improvement when losses in the resonating nodes are considered (lossless example: $\Omega_0 = 0$, $\Omega_z = 5.5$, $M_{1,2} = M_{11,12} = 1.9325$, and $M_{6,7} = 1.8281$; lossy example: $\Omega_0 = -0.2j$, $M_{4,4} = M_{9,9} = -5.5 - 0.2j$, $M_{5,5} = M_{10,10} = 5.5 - 0.2j$, $M_{1,2} = M_{11,12} = 1.9325$, and $M_{6,7} = 1.8281$; compensated lossy example: $\Omega_0 = -0.2j$, $M_{4,4} = M_{9,9} = -5.5 - 0.2j$, $M_{5,5} = M_{10,10} = 5.5 - 0.2j$, $M_{1,2} = M_{11,12} = 2.21$, and $M_{6,7} = 1.277$). (a) $|S_{21}|$ and $|S_{11}|$. (b) $|S_{21}|$ (passband detail).

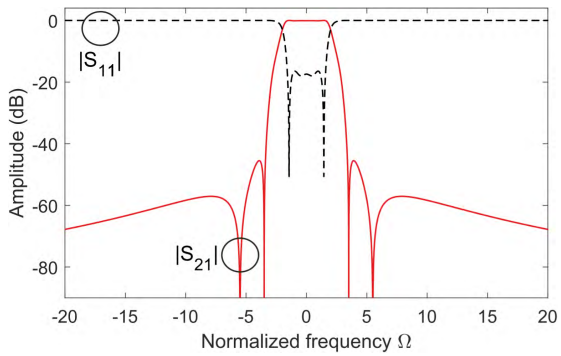

FIGURE 7. Theoretical power transmission ($|S_{21}|$) and reflection ($|S_{11}|$) parameters for a four-TZ state of the two-stage ($K = 2$) adaptive-bandwidth/enhanced-in-band-flatness BPF architecture in Fig. 4 ($M_{4,4} = -M_{5,5} = -5.5$, $M_{9,9} = -M_{10,10} = -3.5$, $M_{1,2} = M_{11,12} = 1.6838$, and $M_{6,7} = 1.4378$).

admittance-inverter and resonator implementations adopted in each case, different out-of-band stopband-attenuation characteristics are obtained for each of them. In particular, Fig. 8(a) and (b) show two distinct high-frequency BPF circuit networks that can be modeled with the one-stage ($K = 1$) coupling-routing diagram in Fig. 2, as follows (f_0 is the center frequency and f_{z1} and f_{z2} the lower and upper TZ frequencies):

- The circuit in Fig. 8(a) consists of the direct matching of the one-stage coupling-routing diagram in Fig. 2. Here, the admittance inverters are designed as quarter-wavelength-at-f_0 transmission-line segments and the outermost resonators and the ones in the TZ-creation cell as capacitively-loaded transmission-line segments that are half-wavelength long at f_0, f_{z1}, and f_{z2}, respectively.
- The circuit in Fig. 8(b) corresponds to a simplified version in which some of the inter-resonator admittance inverters are absorbed with part of the capacitively-loaded transmission-line resonators, whereas the input/output admittance inverters are realized with capacitors.

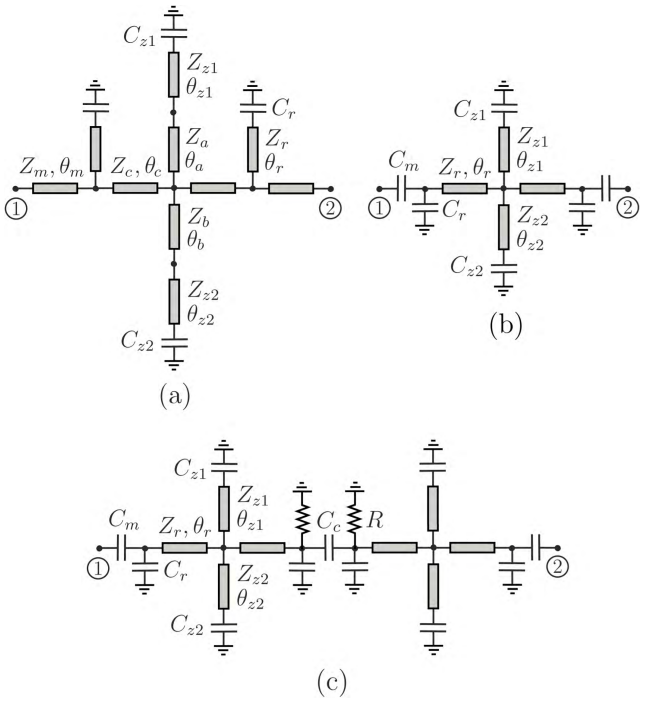

FIGURE 8. Capacitively-loaded transmission-line BPF realizations of the coupling-routing diagram in Fig. 1. (a) Direct-matching realization ($K = 1$). (b) Simplified realization ($K = 1$). (c) Two-stage ($K = 2$) realization based on the in-series cascade of two replicas of the BPF stage in Fig. 8(b).

For illustration purposes, Fig. 9 compares the theoretical power transmission and reflection parameters of the BPF circuits in Fig. 8(a) and (b) for example designs with the same 3-dB absolute bandwidth. As can be seen, the BPF structure in Fig. 8(b) demonstrates broader lower and upper stopband bandwidths due to the absence of close-to-passband spurious transmission ranges. Moreover, the employment of capacitors in both the resonators and the external admittance inverters is a preferred option to make them adjustable for bandwidth/amplitude-flatness-tuning purposes by means of variable-reactance elements in a real BPF implementation.

On the other hand, Fig. 8(c) depicts the detail of the cascade of two replicas of the circuit network in Fig. 8(b) for higher-order/selectivity realizations. Note that the two constituent stages are connected by means of a capacitive-type admittance inverter and two grounded resistors. As proven in Fig. 10 in which the theoretical power transmission and

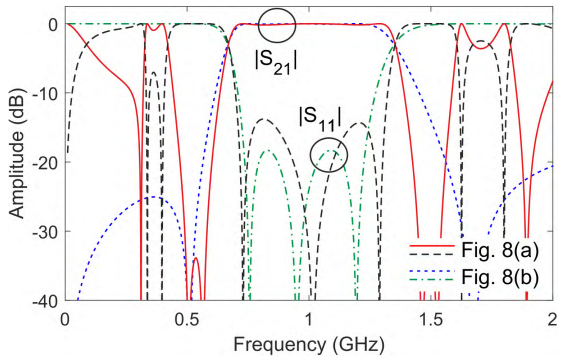

FIGURE 9. Examples of theoretical power transmission ($|S_{21}|$) and reflection ($|S_{11}|$) parameters of the capacitively-loaded transmission-line BPF networks in Fig. 8(a) and (b) (Fig. 8(a): $Z_0 = 50\ \Omega$, $f_0 = 1$ GHz, $Z_{z1} = 50\ \Omega$, $Z_{z2} = 50\ \Omega$, $Z_r = 50\ \Omega$, $Z_a = 50\ \Omega$, $Z_b = 50\ \Omega$, $Z_m = 38\ \Omega$, $\theta_a(f_0) = 90^o$, $\theta_b(f_0) = 90^o$, $\theta_m(f_0) = 90^o$, $\theta_r(f_0) = 160^o$, $\theta_{z1}(f_0) = 40^o$, $\theta_{z2}(f_0) = 21^o$, $C_r = 1$ pF, $C_{z1} = 12$ pF, and $C_{z2} = 2.9$ pF; Fig. 8(b): $Z_0 = 50\ \Omega$, $f_0 = 1$ GHz, $Z_{z1} = 45\ \Omega$, $Z_{z2} = 45\ \Omega$, $Z_r = 60\ \Omega$, $\theta_r(f_0) = 41^o$, $\theta_{z1}(f_0) = 35^o$, $\theta_{z2}(f_0) = 16^o$, $C_r = 1$ pF, $C_{z1} = 21.5$ pF, $C_{z2} = 4.18$ pF, and $C_m = 3.6$ pF).

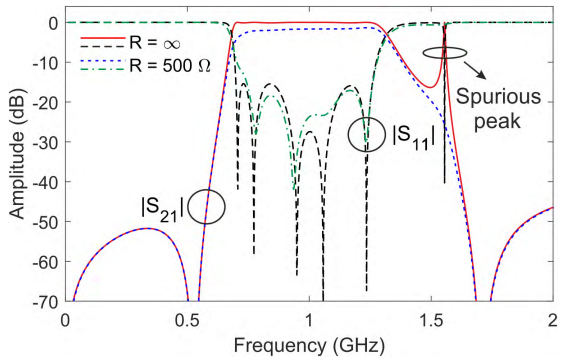

FIGURE 10. Examples of theoretical power transmission ($|S_{21}|$) and reflection ($|S_{11}|$) parameters of the two-stage capacitively-loaded transmission-line BPF in Fig. 8(c) with/without resistors in the inter-stage cascading section ($Z_0 = 50\ \Omega$, $f_0 = 1$ GHz, $Z_r = 60\ \Omega$, $Z_{z1} = 45\ \Omega$, $Z_{z2} = 45\ \Omega$, $\theta_r(f_0) = 41^o$, $\theta_{z1}(f_0) = 35^o$, $\theta_{z2}(f_0) = 16^o$, $C_r = 1$ pF, $C_{z1} = 20$ pF, $C_{z2} = 4$ pF, $C_m = 3.6$ pF, and $C_c = 1.7$ pF).

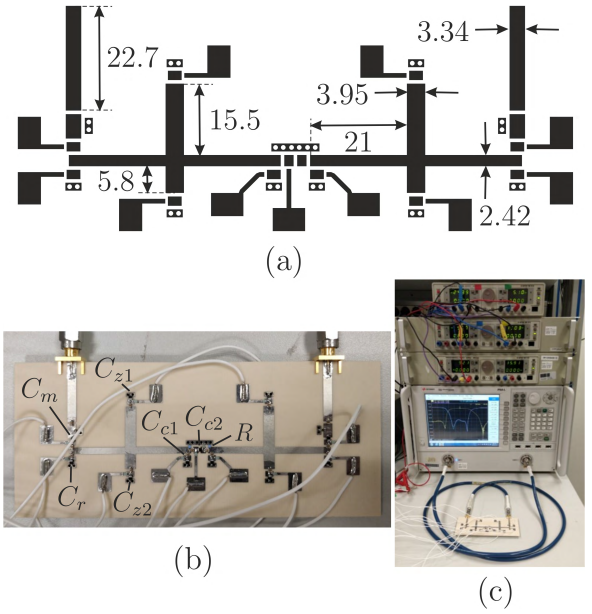

FIGURE 11. Manufactured electronically-controllable microstrip prototype of the two-stage bandwidth-reconfigurable sharp-rejection BPF with enhanced in-band amplitude flatness. (a) Layout (dimensions, in mm, are indicated). (b) Photograph (core size: 120 × 40.2 mm^2; weight: 34 gr). (c) Experimental set-up.

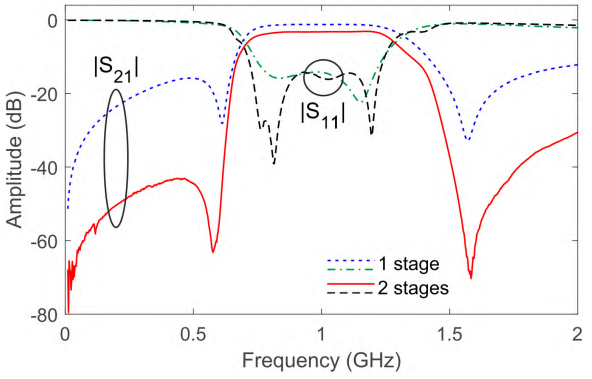

FIGURE 12. Measured power transmission ($|S_{21}|$) and reflection ($|S_{11}|$) responses for one illustrative wide-band state of the manufactured electronically-controllable microstrip prototype of the two-stage bandwidth-reconfigurable sharp-rejection BPF with enhanced in-band amplitude flatness—in comparison with those of its constituent stage.

reflection responses of an example design of the two-stage BPF circuit in Fig. 8(c) are shown, these resistors allow to suppress the undesired out-of-band upper spike resulting from the cascading process between the two stages. Nevertheless, this is done at the expense of increased in-band insertion-loss levels (increase of the minimum in-band insertion-loss level by 1.3 dB in this example) but while reasonably maintaining the in-band amplitude-flatness performance of the overall BPF.

III. EXPERIMENTAL RESULTS

To validate the practical usefulness of the proposed concept of bandwidth-reconfigurable sharp-rejection BPF with enhanced in-band amplitude flatness, a proof-of-concept electronically-controllable prototype has been manufactured in microstrip technology and tested. It corresponds to the two-stage BPF architecture in Fig. 8(c) for a center frequency of 1 GHz and a 1-dB-referred bandwidth variation from 36 MHz to 500 MHz—i.e., from 3.6% to 50% in relative terms—that corresponds to a unprecedented bandwidth-tuning ratio of 13.9:1 between narrow-band and ultra-wideband states.

The layout and a photograph of the manufactured BPF circuit and the experimental set-up that was arranged for its characterization are shown in Fig. 11. For its development, an RO4003C microstrip substrate with the following characteristics was used: relative dielectric permittivity $\varepsilon_r = 3.38$ (± 0.05), dielectric thickness $H = 1.524$ mm, metal thickness $t = 17.8\ \mu$m, and dielectric loss tangent $\tan(\delta_D) = 0.0027$. For the variable capacitors in the resonators of the TZ-creation cells—i.e., C_{z1} and C_{z2} in Fig. 8(c)—, varactor

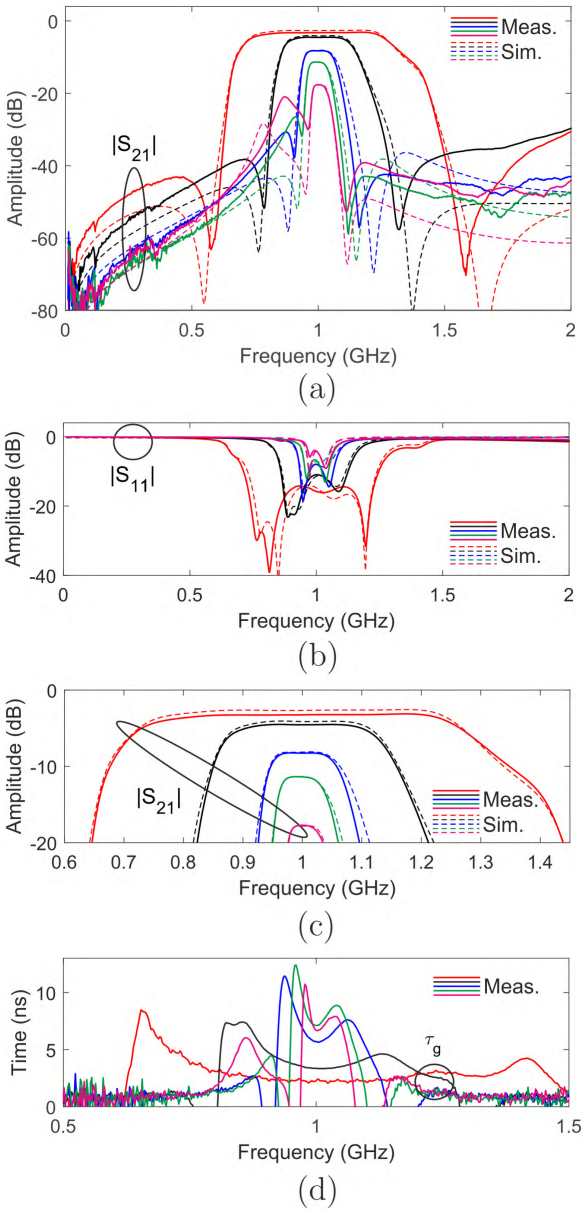

FIGURE 13. Simulated and measured power transmission ($|S_{21}|$) and reflection ($|S_{11}|$) responses and measured group-delay (τ_g) responses corresponding to five bandwidth states around 1 GHz of the manufactured electronically-controllable microstrip prototype of the two-stage bandwidth-reconfigurable sharp-rejection BPF with enhanced in-band amplitude flatness: states with two double TZs. (a) $|S_{21}|$. (b) $|S_{11}|$. (c) $|S_{21}|$ (passband detail). (d) τ_g.

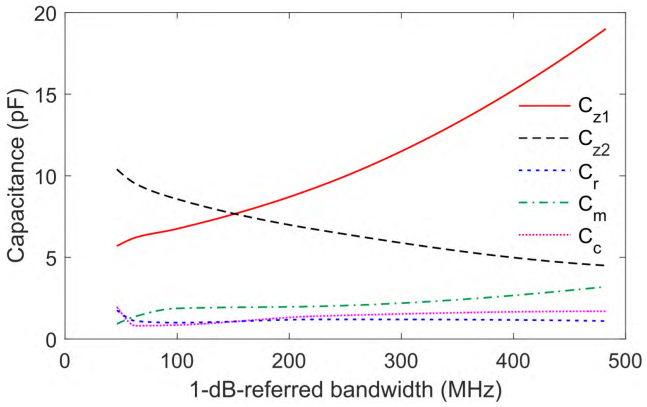

FIGURE 14. Capacitance-variation curves for the variable capacitors of the manufactured electronically-controllable microstrip prototype of the two-stage bandwidth-reconfigurable sharp-rejection BPF with enhanced in-band amplitude flatness—extracted from the simulations.

diodes model BB545 from Infineon with 2-20-pF range were used, whereas the remaining controllable capacitors—i.e., C_r, C_m, and C_c in Fig. 8(c)—were realized with varactor diodes model BB837 from Infineon with 0.52-6.6-pF range. Note that the capacitors C_r in the outermost resonators were also made tunable to have further capability to compensate experimental deviations. For the biasing networks of these varactors, RF-block resistors of 10 kΩ and DC-isolation capacitors of 10 nF were utilized. Furthermore, in the inter-stage cascading inverter and as it was detailed in Section II.B, resistors of 500 Ω—R in Fig. 8(c)—were employed to suppress undesired spurious peaks caused by the inter-stage cascading process at the expense of some additional power insertion loss. The ground connections for the varactor diodes and the resistors were realized by means of 1-mm-diameter via holes.

The measured power transmission and reflection responses of the constructed prototype for one example wide-band state in comparison with those of its constituent stage—which was also fabricated—are depicted in Fig. 12. As can be seen, a noticeable selectivity increase when compared to the single stage is obtained for the overall two-stage BPF circuit.

The tuning capabilities of this prototype are illustrated in Fig. 13, which depicts its simulated and measured power transmission and reflection responses and measured in-band group-delay curves for five different bandwidth states with flattened passband centered at 1 GHz and double lower and upper TZs—i.e., five different biasing voltages in the filter—. As can be seen, a fairly-close agreement between experimental and predicted results is obtained in all cases. The main characteristics for these measured responses are as follows—listed from the widest- to the narrowest-bandwidth state, respectively—: 1-dB-referred absolute bandwidth of 482.2 MHz, 224.6 MHz, 98.1 MHz, 63.1 MHz, and 46.2 MHz—i.e., 44.22%, 22.46%, 9.81%, 6.31%, and 4.62% in relative terms—, minimum in-band power-insertion-loss level equal to 3.12 dB, 4.5 dB, 8.24 dB, 11.36 dB, and 17.7 dB, minimum in-band power-matching level of 14.2 dB, 11 dB, 7.9 dB, 6.6 dB, and 4 dB, and maximum group-delay variation within the measured 1-dB-referred bandwidth equal to 1.8 ns, 2.3 ns, 3.9 ns, 3.6 ns, and 4.1 ns. Note that these results experimentally confirm how the passband flattening is attained at the expense of higher in-band power-reflection loss, where 46.2 MHz was the minimum 1-dB bandwidth state for which such flattening was experimentally verified due to the granularity—i.e., limitation in the very-fine tuning—of the varactor elements. Moreover, the minimum in-band power-matching level

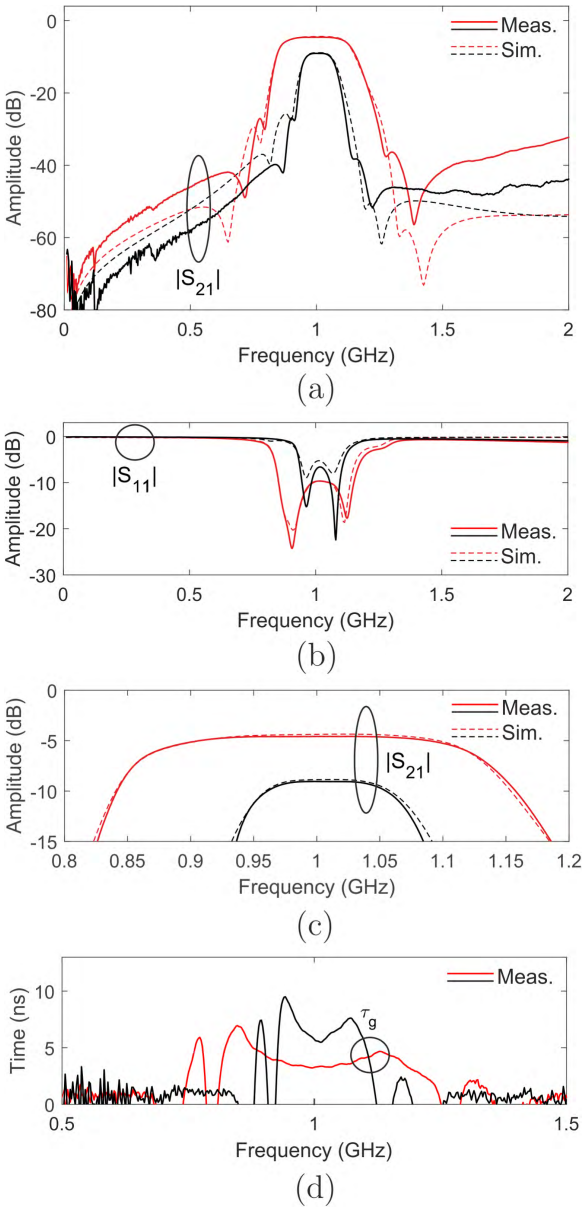

FIGURE 15. Simulated and measured power transmission ($|S_{21}|$) and reflection ($|S_{11}|$) responses and measured group-delay (τ_g) responses corresponding to two bandwidth states around 1 GHz of the manufactured electronically-controllable microstrip prototype of the two-stage bandwidth-reconfigurable sharp-rejection BPF with enhanced in-band amplitude flatness: states with four simple TZs. (a) $|S_{21}|$. (b) $|S_{11}|$. (c) $|S_{21}|$ (passband detail). (d) τ_g.

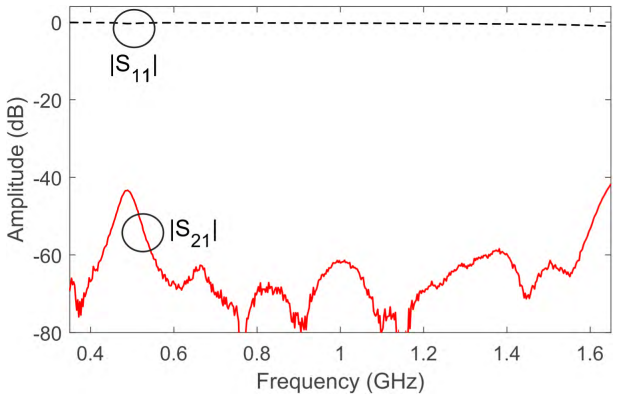

FIGURE 16. Measured intrinsic-switching-off state in terms of measured power transmission ($|S_{21}|$) and reflection ($|S_{11}|$) responses of the manufactured electronically-controllable microstrip prototype of the two-stage bandwidth-reconfigurable sharp-rejection BPF with enhanced in-band amplitude flatness.

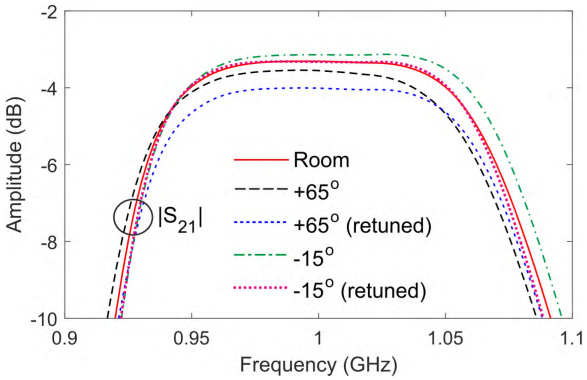

FIGURE 17. Measured power transmission responses ($|S_{21}|$) for the individual stage of the manufactured electronically-controllable microstrip prototype of the two-stage bandwidth-reconfigurable sharp-rejection BPF with enhanced in-band amplitude flatness: state of 250-MHz 1-dB-referred bandwidth for room, $+65^{o}$ C, and -15^{o} C temperatures (the recovered flattened responses after the retuning/restoring process are also included).

of 4 dB in this case is in concordance to what is commonly observed in classic frequency-static predistorted filter designs (e.g., see [3, Fig. 12]). Fig. 14 represents the variation of the tunable-capacitance values as extracted from the simulated responses, so that their tuning trends as a function of the required 1-dB-referred absolute bandwidth can be observed.

To further demonstrate the flexibility of the experimental prototype of the two-stage bandwidth-reconfigurable sharp-rejection BPF with enhanced in-band amplitude flatness, two flattened-passband states showing four TZs with two different TZs at each passband side are plotted in Fig. 15—i.e., seven different biasing voltages in the filter—. They reveal how the TZs of each stage can be set in an independent way to configure more-general out-of-band power-rejection profiles. Specifically, these two states exhibit 1-dB-referred absolute bandwidth of 225.5 MHz and 95.3 MHz—i.e., 22.5% and 9.53% in relative terms—, minimum in-band power-insertion-loss levels equal to 4.6 dB and 9 dB, minimum in-band power-matching level of 9.6 and 6.6 dB, and maximum group-delay variation in the measured 1-dB-referred bandwidth below 1.57 ns and 3.2 ns, respectively. Furthermore, Fig. 16 proves how the filter passband can be intrinsically switched-off—i.e., without RF switches—in the represented 0.35–1.65-GHz range through the detuning of the varactor elements of the filter, so that a minimum power-isolation level of 41.5 dB is attained in this spectral interval.

Finally, the robustness of the manufactured bandwidth/amplitude-flatness-reconfigurable BPF prototype to operate in various temperature conditions was tested. Specifically, for its single stage, Fig. 17 represents the measured power transmission responses—in-band detail—of this circuit for three distinct temperatures as follows: room, $+65^{o}$ C, and -15^{o} C. As shown, the passband power-insertion-loss levels and amplitude flatness are deteriorated as the temperature gets higher. However, such undesired effect can be compensated by restoring the amplitude-flatness performance of the filter with the fine retuning of its external quality factor and poles.

IV. CONCLUSION

A broadly-controllable sharp-rejection BPF with ultra-large electronic-bandwidth-tuning ratio and passband-flattening capabilities has been presented. It is based on a multi-resonator cascade arrangement in which the bandwidth reconfiguration is realized through the tuning of those resonators that produce TZs. The in-band flattening is carried out by controlling the external and inter-BPF-stage admittance inverters in basis to an in-band frequency-selective signal-reflection process. The operational foundations of this reconfigurable BPF concept in terms of coupling-routing diagram and a capacitively-loaded transmission-line-based realization for it have been detailed. Undesired effects inherent to such distributed-element resonator-cascade realization, such as the appearance of out-of-band spikes, are mitigated with the inclusion of resistive elements in the inter-stage admittance inverters. For practical-demonstration purposes, a 1-GHz six-pole BPF prototype with four TZs that are grouped in pairs has been developed and measured. It features continuously-selectable flattened bandwidths from 42 MHz to 482 MHz—i.e., measured bandwidth-tuning ratio of 11.5:1—, intrinsic-switching-off capabilities by means of resonator detuning, and passband-flatness restoring for different temperature conditions.

REFERENCES

[1] H. Chan, "Advanced microwave technologies for smart flexible satellite," in *IEEE MTT-S Int. Microw. Symp. Dig.* Baltimore, MD, USA, Jun. 2011, pp. 1–4.
[2] H. Maune *et al.*, "Tunable microwave component technologies for SatCom-platforms," in *Proc. German Microw. Conf.*, Bochum, Germany, Mar. 2016, pp. 23–26.
[3] A. C. Guyette, I. C. Hunter, and R. D. Pollard, "The design of microwave bandpass filters using resonators with nonuniform Q," *IEEE Trans. Microw. Theory Techn.*, vol. 54, no. 11, pp. 3914–3922, Nov. 2006.
[4] J. Mateu *et al.*, "Synthesis of 4th order lossy filters with uniform *Q* distribution," in *IEEE MTT-S Int. Microw. Symp. Dig.*, Anaheim, CA, USA, May 2010, p. 1.
[5] A. Basti, A. Périgaud, S. Bila, S. Verdeyme, L. Estagerie, and H. Leblond, "Design of microstrip lossy filters for receivers in satellite transponders," *IEEE Trans. Microw. Theory Techn.*, vol. 62, no. 9, pp. 2014–2024, Sep. 2014.
[6] L.-F. Qiu, L.-S. Wu, W.-Y. Yin, and J.-F. Mao, "A flat-passband microstrip filter with nonuniform-*Q* dual-mode resonators," *IEEE Microw. Wireless Compon. Lett.*, vol. 26, no. 3, pp. 183–185, Mar. 2016.
[7] M. Meng, I. C. Hunter, and J. D. Rhodes, "The design of parallel connected filter networks with nonuniform *Q* resonators," *IEEE Trans. Microw. Theory Techn.*, vol. 61, no. 1, pp. 372–381, Jan. 2013.
[8] C. Rauscher, "Reconfigurable bandpass filter with a three-to-one switchable passband width," *IEEE Trans. Microw. Theory Techn.*, vol. 51, no. 2, pp. 573–577, Feb. 2003.
[9] C. Lugo, D. Thompson, and J. Papapolymerou, "Reconfigurable bandpass filter with variable bandwidth at 5.8 GHz using a capacitive gap variation technique," in *Proc. 33rd Eur. Microw. Conf.*, Munich, Germany, vol. 3, Oct. 2003, pp. 923–926.
[10] M. Sanchez-Renedo, R. Gomez-Garcia, J. Alonso, and C. Briso-Rodriguez, "Tunable combline filter with continuous control of center frequency and bandwidth," *IEEE Trans. Microw. Theory Techn.*, vol. 53, no. 1, pp. 191–199, Jan. 2005.
[11] A. C. Guyette, "Alternative architectures for narrowband varactor-tuned bandpass filters," in *Proc. 39th Eur. Microw. Conf.*, Rome, Italy, vol. 2, Sep. 2009, pp. 475–478.
[12] C.-C. Cheng and G. M. Rebeiz, "High-*Q* 4–6-GHz suspended stripline RF MEMS tunable filter with bandwidth control," *IEEE Trans. Microw. Theory Techn.*, vol. 59, no. 10, pp. 2469–2476, Oct. 2011.
[13] Y.-C. Chiou and G. M. Rebeiz, "A tunable three-pole 1.5–2.2-GHz bandpass filter with bandwidth and transmission zero control," *IEEE Trans. Microw. Theory Techn.*, vol. 59, no. 11, pp. 2872–2878, Nov. 2011.
[14] T. Yang and G. M. Rebeiz, "Tunable 1.25–2.1-GHz 4-pole bandpass filter with intrinsic transmission zero tuning," *IEEE Trans. Microw. Theory Techn.*, vol. 63, no. 5, pp. 1569–1578, May 2015.
[15] P. Wong and I. C. Hunter, "Electronically reconfigurable microwave bandpass filter," *IEEE Trans. Microw. Theory Techn.*, vol. 57, no. 12, pp. 3070–3079, Dec. 2009.
[16] M. A. Sánchez-Soriano, R. Gómez-García, G. Torregrosa-Penalva, and E. Bronchalo, "Reconfigurable-bandwidth bandpass filter within 10-50%," *IET Microw. Antennas Propag.*, vol. 7, no. 7, pp. 502–509, May 2013.
[17] K. Rabbi and D. Budimir, "Miniaturised sharp rejection bandpass filter with reconfigurable bandwidth for UWB applications," in *Proc. 43rd Eur. Microw. Conf.*, Nuremberg, Germany, Oct. 2013, pp. 1023–1026.
[18] C. H. Kim and K. Chang, and X. Liu, "Varactor tuned ring resonator filter with wide tunable bandwidth," in *Proc. IEEE Radio Wireless Symp.*, San Diego, CA, USA, Jan. 2015, pp. 141–143.
[19] J.-R. Mao, W.-W. Choi, K.-W. Tam, W. Q. Che, and Q. Xue, "Tunable bandpass filter design based on external quality factor tuning and multiple mode resonators for wideband applications," *IEEE Trans. Microw. Theory Techn.*, vol. 61, no. 7, pp. 2574–2584, Jul. 2013.
[20] J. Cai, W. Qin, J.-X. Chen, and Q. Xue, "Novel varactor-tuned coupling mechanism and its applications to high-order bandwidth-agile bandpass filters," *IEEE Trans. Compon., Packag., Manuf. Technol.*, vol. 7, no. 2, pp. 246–253, Feb. 2017.
[21] D. Psychogiou, R. Gómez-García, and D. Peroulis, "Adaptive-transfer-function bandpass filters using reconfigurable evanescent-mode-cavity resonator cascades," in *IEEE MTT-S Int. Microw. Symp. Dig.*, San Francisco, CA, USA, May 2016, pp. 1–4.
[22] R. Gómez-García, J.-M. Muñoz-Ferreras, and D. Psychogiou, "Fully-reconfigurable bandpass filter with static couplings and intrinsic-switching capabilities," in *IEEE MTT-S Int. Microw. Symp. Dig.*, Honolulu, HI, USA, Jun. 2017, pp. 914–917.
[23] D. J. Simpson, R. Gómez-García, and D. Psychogiou, "UHF-band bandpass filters with fully-reconfigurable transfer function," in *Proc. Int. Symp. Appl. Comput. Electromagn. Soc. (ACES)*, Denver, CO, USA, Mar. 2018, pp. 1–2.
[24] D. J. Simpson, R. Gómez-García, and D. Psychogiou, "Planar RF duplexer with multiple levels of transfer-function reconfigurability," in *Proc. 48th Eur. Microw. Conf.*, Madrid, Spain, Sep. 2018, pp. 535–538.
[25] J. Ni and J. Hong, "Varactor-tuned microstrip bandpass filters with different passband characteristics," *IET Microw., Antennas Propag.*, vol. 8, no. 6, pp. 415–422, Apr. 2014.
[26] R. Gómez-García, J.-M. Muñoz-Ferreras, J. Jiménez-Campillo, L. Arche-Andradas, F. Branca-Roncati, and P. Martín-Iglesias, "Electronically-controllable bandpass planar filter with ultra-large bandwidth-tuning ratio and enhanced in-band amplitude flatness," in *Proc. 48th Eur. Microw. Conf.*, Madrid, Spain, Sep. 2018, pp. 543–546.
[27] S. Morini, G. Venanzoni, P. M. Iglesias, C. Ernst, A. Di Donato, and M. Farina, "Systematic evaluation of spikes due to interference between cascaded filters," *IEEE Trans. Microw. Theory Techn.*, vol. 66, no. 11, pp. 4814–4819, Nov. 2018.

ROBERTO GÓMEZ-GARCÍA (S'02–M'06–SM'11) was born in Madrid, Spain, in 1977. He received the Telecommunication Engineering and Ph.D. degrees from the Polytechnic University of Madrid, Madrid, in 2001 and 2006, respectively. Since 2006, he has been an Associate Professor with the Department of Signal Theory and Communications, University of Alcalá, Alcalá de Henares, Spain. He has had several research stays with the C2S2 Department, XLIM Research Institute, University of Limoges, Limoges, France; Telecommunications Institute, University of Aveiro, Aveiro, Portugal; U.S. Naval Research Laboratory, Microwave Technology Branch, Washington, DC, USA; and Purdue University, West Lafayette, IN, USA. He is currently an Adjunct Part-Time Professor with the University of Electronic Science and Technology of China, Chengdu, China. His current research interests include the design of fixed/tunable high-frequency filters and multiplexers in planar, hybrid, and monolithic microwave integrated circuit technologies, multifunction circuits and systems, software-defined radio and radar architectures for telecommunications, and remote sensing and biomedical applications.

Dr. Gómez-García serves as a member for the Technical Review Board of several IEEE and EuMA conferences, the IEEE MTT-S Microwave Acoustics Committee (MTT-2), the IEEE MTT-S Filters and Passive Components Committee (MTT-8), the IEEE MTT-S Biological Effect and Medical Applications of RF and Microwave Committee (MTT-10), the IEEE MTT-S Wireless Communications Committee (MTT-20), and the IEEE CAS-S Analog Signal Processing Technical Committee. He was a recipient of the 2016 IEEE MTT-S Outstanding Young Engineer Award. He was an Associate Editor of the IEEE TRANSACTIONS ON MICROWAVE THEORY AND TECHNIQUES, from 2012 to 2016, and the IEEE TRANSACTIONS ON CIRCUITS AND SYSTEMS-I: REGULAR PAPERS, from 2012 to 2015, and a Senior Editor of the IEEE JOURNAL ON EMERGING AND SELECTED TOPICS IN CIRCUITS AND SYSTEMS, from 2016 to 2017. He was a Guest Editor of the IEEE JOURNAL ON EMERGING AND SELECTED TOPICS IN CIRCUITS AND SYSTEMS 2013 Special Issue on Advanced Circuits and Systems for CR/SDR Applications, the *IET Microwaves, Antennas, and Propagation* 2013 Special Issue on Advanced Tunable/Reconfigurable and Multi-Function RF/Microwave Filtering Devices, and *IEEE Microwave Magazine* 2014 Special Issue on Recent Trends on RF/Microwave Tunable Filter Design. He is currently an Associate Editor of the IEEE JOURNAL OF ELECTROMAGNETICS, RF AND MICROWAVES IN MEDICINE AND BIOLOGY, the IEEE ACCESS, *IET Microwaves, Antennas, and Propagation*, and the *International Journal of Microwave and Wireless Technologies*. He is a Reviewer for several IEEE, IET, EuMA, and Wiley publications.

JOSÉ-MARÍA MUÑOZ-FERRERAS (M'15) was born in Madrid, Spain, in 1981. He received the degree in telecommunication engineering and the Ph.D. degree in electrical and electronic engineering from the Polytechnic University of Madrid, Spain, in 2004 and 2008, respectively. He is currently an Associate Professor with the Department of Signal Theory and Communications, University of Alcalá, Alcalá de Henares, Spain. His current research interests include radar signal processing, advanced radar systems and concepts, and microwave/radio frequency (RF) circuits and systems, specifically focusing on high-resolution inverse synthetic aperture radar images, and the design and validation of radar systems for short-range applications.

Dr. Muñoz-Ferreras serves as a member for the Technical Review Board of the IEEE MTT-S International Microwave Symposium, the IEEE International Geoscience and Remote Sensing Symposium, the IEEE Radar Conference, and the European Radar Conference. He is also a member of the IEEE MTT-S Biological Effects and Medical Applications of RF and Microwave (MTT-10) Technical Committee. He is a Reviewer for several IEEE and IET publications.

JESÚS JIMÉNEZ-CAMPILLO was born in Murcia, Spain, in 1987. He received the Telecommunication Engineering degree from the Technical University of Cartagena, Cartagena, Spain, in 2010.

He was with Filtronic, Britain, where he was involved in designing radio frequency (RF) passive components for the mobile telecommunications industry, and also with the Electronic Technologies and Radiofrequency Department, National Institute of Aerospace Technology, Spain. He is currently an RF Engineer with Thales Alenia Space, Spain, where he is also the Technical Responsible Engineer for passive RF projects of different satellite programs. He is involved in research projects of additive manufacturing for passive components and tunable high-frequency filters. His entire professional career has been performed within the RF sector.

FEDERICO BRANCA-RONCATI was born in Buenos Aires, Argentina, in 1978. He received the Telecommunication Engineering degree from the Polytechnic University of Madrid, Madrid, Spain, in 2003.

He was a Technical Responsible Engineer for passive radio frequency (RF) projects of different satellite programs and responsible for research and development activities for various technologies. Since 2003, he has been with Thales Alenia Space, Spain, where he is involved in space business activities. He has been a Project Manager for the last three years and leading the projects of passive and active RF equipment and sub-systems for different satellite programs and research projects. He has been an RF Engineer with Thales Alenia Space, for 13 years. His research was focused on dielectric resonators technologies for input and output multiplexers.

PETRONILO MARTÍN-IGLESIAS was born in Cáceres, Spain, in 1980. He received the Telecommunication Engineering degree from the Polytechnic University of Madrid, Madrid, Spain, in 2002, and the master's degree from the University of Leeds, Leeds, U.K., in 2012.

He was a Microwave Engineer with industry for more than 15 years for active (high power amplifiers for radar applications) and passive (filters, multiplexers, and couplers) radio frequency (RF) hardware design. He was a Radar System Engineer with Indra Sistemas, ISDEFE S.A., and Thales Alenia Space, Spain, for two years. Since 2012, he has been with the European Space Agency, Paris, France, where he is involved in research and development and project support activities related to RF passive hardware developments. His current research interests include filter synthesis theory, electromagnetic design, high-power prediction, and advanced manufacturing techniques for RF passive hardware.